

LETTERS

Infinite-layer iron oxide with a square-planar coordination

Y. Tsujimoto¹, C. Tassel^{1,2}, N. Hayashi³, T. Watanabe¹, H. Kageyama¹, K. Yoshimura¹, M. Takano^{4,5}, M. Ceretti², C. Ritter⁶ & W. Paulus²

Conventional high-temperature reactions limit the control of coordination polyhedra in transition-metal oxides to those obtainable within the bounds of known coordination geometries for a given transition metal¹. For example, iron atoms are almost exclusively coordinated by three-dimensional polyhedra such as tetrahedra and octahedra. However, recent works have shown that binary metal hydrides act as reducing agents at low temperatures, allowing access to unprecedented structures^{2–4}. Here we show the reaction of a perovskite SrFeO₃ with CaH₂ to yield SrFeO₂, a new compound bearing a square-planar oxygen coordination around Fe²⁺. SrFeO₂ is isostructural with ‘infinite layer’ cupric oxides^{5–8}, and exhibits a magnetic order far above room temperature in spite of the two-dimensional structure, indicating strong in-layer magnetic interactions due to strong Fe *d* to O *p* hybridization. Surprisingly, SrFeO₂ remains free from the structural instability that might well be expected at low temperatures owing to twofold orbital degeneracy in the Fe²⁺ ground state with D_{4h} point symmetry. The reduction and the oxidation between SrFeO₂ and SrFeO₃ proceed via the brownmillerite-type intermediate SrFeO_{2.5}, and start at the relatively low temperature of ~400 K, making the material appealing for a variety of applications, including oxygen ion conduction, oxygen gas absorption and catalysis.

The coordination number in ionically bonded structures is governed by the relative size of oppositely charged ions, which to a first approximation may be regarded as charged rigid spheres (Pauling’s first rule)¹. Each ion ‘tries’ to surround itself symmetrically with the largest possible number of oppositely charged neighbours. Transition metal ions normally have, owing to their relatively small ionic radii, a preference for tetrahedral and octahedral coordination, as found typically in perovskites and spinels.

For an octahedral coordination there is a pronounced effect on the stereochemistry, or a substantial deviation from ideal geometry, for the Jahn–Teller ions with (*e_g*)¹ or (*e_g*)³ configuration, such as Cr²⁺, Mn³⁺ (*d*⁴) and Cu²⁺, Ni²⁺ (*d*⁸), in which the lengthening of a pair of bonds perpendicular to the equatorial plane gives a tetragonal distortion (*c/a* > 1) and results ultimately in a square-planar coordination¹. Among many copper oxides with square planar geometry, the series ACuO₂ (where A = Sr, Ca)^{5,6} are known as the “infinite-layer compounds”, or the mother structure of high-temperature (*T_c*) superconductors^{7,8}, which consist of a sequence of infinitely repeating stacking of CuO₂ square lattices. The isostructural phase of LaNiO₂ is formed naturally because monovalent nickel is isoelectronic with divalent copper⁹. Unusual coordination beyond the constraint of the ionic model may occur in association with covalent bonding, which is highly directional, as realized, for example, in many silicates and sulphides¹⁰. A successful approach

for exploring unusual coordinations in molecular compounds is the use of organic ligands with specific steric constraints^{11,12}. This cannot be applied, however, to nonmolecular inorganic solids.

Iron, one of the richest elements in the Earth, forms an uncountable number of oxides, some of which have been widely used in industry as low-cost ferrite magnets and pigments. In almost all of them, the iron ions are tetrahedrally or octahedrally coordinated. To the best of our knowledge, the only example of square-planar coordination is represented by the mineral gillespite BaFeSi₄O₁₀ (ref. 13). However, the iron atoms in this oxide are dispersed separately within the building blocks made of four-membered rings of SiO₄^{4–} tetrahedra, rendering the electromagnetic properties of minor interest. Ordered perovskites CaFe₃Ti₄O₁₂ and CaFeTi₂O₆ have also been discussed as synthetic examples of the square planar geometry¹⁴, but they actually have four short (~2.0 Å) and four long (~2.8 Å) Fe–O bonds, resulting in a three-dimensional environment.

Here we show a low-temperature route for the topotactic synthesis of a new infinite-layer iron oxide, SrFeO₂ (Fig. 1b), using an easy-to-prepare, slightly oxygen-deficient perovskite SrFeO_{3–*y*} (*y* ≈ 0.125) as a precursor (Fig. 1a). The formation of the strongly anisotropic framework of SrFeO₂ is remarkable in that (1) the Jahn–Teller effect should not be of essential importance for divalent iron ions, (2) such an unusual geometry is obtained for a simple ionic compound, and (3) unlike BaFeSi₄O₁₀, the FeO₂ layers form the primary building blocks, making it a quasi-two-dimensional magnet. Furthermore, the oxygen content in AFeO_{3–*y*} (A = Sr, Ca) has been taken for granted to be in the range of only 0 ≤ *y* ≤ 0.5, and thus the brownmillerite phase SrFeO_{2.5} (*y* = 0.5) (see Supplementary Fig. 1), consisting of alternative layers of FeO₆ octahedra and FeO₄ tetrahedra, was historically assumed to represent the lower limit of oxygen stoichiometry. This is in spite of extensive experimental efforts to control oxygen content that include synthesis at high temperature with oxygen partial pressures ranging from 10^{–9} to 100 MPa (refs 15, 16), electrochemical reactions in aqueous solution at room temperature¹⁷, and the fabrication of epitaxial films under different atmospheres¹⁸.

Our approach follows the recent success in the use of hydrides of electropositive metals as powerful reducing agents^{2–4,19–22} such as NaH and CaH₂. For example, using NaH yields LaSrCoO_{3.38} from LaSrCoO₄ (ref. 2) and YSr₂Mn₂O_{5.5} from YSr₂Mn₂O₇ (ref. 19), and using CaH₂ yields LaSrCoO₃H_{0.7} from LaSrCoO₄ (ref. 3), Yb₂Ti₂O_{6.43} from Yb₂Ti₂O₇ (ref. 4), and La₃Ni₂O₆ from La₃Ni₂O₇ (ref. 20). These metal hydrides, routinely used as drying agents in organic synthesis, are now regarded as promising reducing agents for nonmolecular compounds to yield unusual frameworks and coordinations in nonmolecular solids, because they are active at

¹Department of Chemistry, Graduate School of Science, Kyoto University, Sakyo, Kyoto 606-8502, Japan. ²University of Rennes 1, Sciences Chimiques de Rennes UMR CNRS 6226, Campus de Beaulieu Bâtiment 10B, Rennes cedex 35042, France. ³Graduate School of Human and Environmental Studies, Kyoto University, Sakyo, Kyoto 606-8501, Japan. ⁴Institute for Chemical Research, Kyoto University, Uji, Kyoto 611-0011, Japan. ⁵Research Institute for Production Development, 15 Morimoto, Shimogamo, Sakyo, Kyoto 606-0805, Japan. ⁶Institute Laue Langevin, BP 156, 38042, Grenoble, France.

considerably lower temperatures than when conventional techniques are used. They also allow solution chemistry to be avoided. However, their potential for the synthesis of new nonmolecular compounds still seems far from realization.

The powder X-ray diffraction (XRD) patterns of the precursor phase $\text{SrFeO}_{2.875}$ (that is, $\text{Sr}_8\text{Fe}_8\text{O}_{23}$) were assigned as the nearly cubic perovskite phase with $a_p \approx 3.86 \text{ \AA}$, though it in fact had a tetragonal $2a_p \times 2a_p \times 2a_p$ supercell ($I4/mmm$, $a = 10.929 \text{ \AA}$ and $c = 7.698 \text{ \AA}$), consistent with the literature^{15,16}. On the other hand, the synchrotron XRD patterns of the final product (Supplementary Fig. 2) were readily indexed assuming the tetragonal unit cell to have $a = 3.99107(3) \text{ \AA}$ and $c = 3.47481(5) \text{ \AA}$, which is completely different from those of any reported SrFeO_{3-y} ($0 \leq y \leq 0.5$) phases. No extra diffraction lines were detected. Compared with the lattice parameters ($a_p \approx 3.86 \text{ \AA}$) of the precursor, the a axis of the final product is slightly increased, but the c axis is drastically decreased. This implies an anisotropic extraction of oxygen atoms located originally on the c axis.

Furthermore, the similarity of the lattice parameters to those of SrCuO_2 ($a = 3.926 \text{ \AA}$ and $c = 3.432 \text{ \AA}$; ref. 6) and also the fact that no specific extinction rules for reflections could be determined from the diffraction pattern, strongly suggest that the two phases are isostructural in the space group of $P4/mmm$. The Rietveld refinement from the synchrotron data immediately converged to $R_{\text{wp}} = 6.04\%$ and $\chi^2 = 4.41$ along with reasonable individual, isotropic displacement factors for all the atoms, suggesting successful structural analysis. The refinement of the site occupancy factor for oxygen atoms gave 0.994(8), indicating that the occupation of the oxygen ($2f$) position is unity within the standard deviation. Inclusion of oxygen atoms into the apical ($1b$) site did not improve the refinement. The bond valence sum calculations gave valences of +1.92 for Sr and +1.97 for

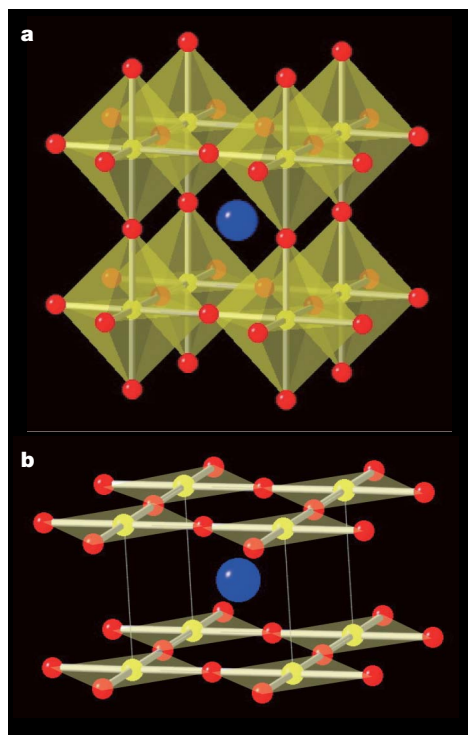


Figure 1 | Structural transformation via a topotactic route. **a**, The cubic perovskite SrFeO_3 . **b**, The infinite-layer compound SrFeO_2 . Iron, strontium and oxygen atoms are represented as yellow, blue and red spheres, respectively. For the sake of simplicity, an idealized and stoichiometric cubic phase, obtainable under high oxygen pressure, is demonstrated in **a**, instead of the distorted, slightly oxygen-deficient phase SrFeO_{3-y} ($y \approx 0.125$) used in this study. The iron coordinations by oxygen atoms are illustrated by octahedra in **a** and squares in **b**.

Fe, which are in excellent agreement with the expected valences of +2 for both. The elemental analysis by energy dispersive spectroscopy (EDS) before and after the reduction gave the same molar ratio of $\text{Sr}:\text{Fe} = 1:1$.

The neutron powder diffraction (NPD) patterns of SrFeO_2 at 293 K (Fig. 2a) confirmed the above structure with an excellent convergence ($R_{\text{wp}} = 4.70\%$ and $\chi^2 = 3.18$). They also excluded a possible incorporation of hydrogen into the structure, and revealed the presence of the (π, π, π) antiferromagnetic order, where the magnetic moments are perpendicular to the c axis (Fig. 2b). This is the same spin structure as that of the undoped, antiferromagnetically ordered mother phase of high- T_c copper oxide superconductors. The magnetic moment has been found to be $3.1\mu_B$ per Fe atom at 293 K and $3.6\mu_B$ at 10 K (Supplementary Fig. 3). The magnitude itself and its minor variation over the wide temperature range strongly suggest that the ferrous ions are in the high-spin state of $(d_{xz} d_{yz})^3 (d_{xy})^1 (d_{z^2})^1 (d_{x^2-y^2})^1$ with $S = 2$ (where S is the magnitude of spin) and that the antiferromagnetic transition temperature is considerably higher than room temperature. The magnetic order at ambient temperature was also confirmed by ^{57}Fe Mössbauer spectroscopy at 285 K (Fig. 3b) showing six well-defined peaks with a fairly large hyperfine field of 40.1 T.

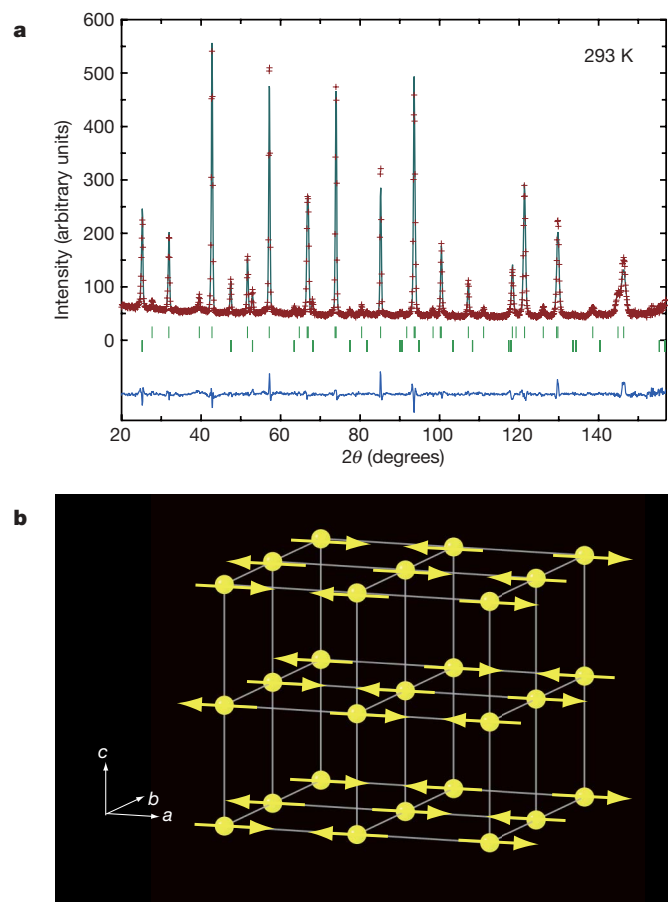


Figure 2 | Structural characterization of SrFeO_2 by Rietveld refinement of high-resolution neutron diffraction at room temperature. **a**, The solid lines and overlying crosses indicate the calculated and observed intensities. The green lines are the positions of the calculated nuclear (top) and magnetic (bottom) Bragg reflections. The difference between the observed and calculated profiles is plotted at the bottom in blue. SrFeO_2 adopts the $P4/mmm$ space group, $a = 3.991(1) \text{ \AA}$, $c = 3.474(1) \text{ \AA}$, Sr on $1d$ (0.5, 0.5, 0.5), Fe on $1a$ (0, 0, 0) and O on $2f$ (0.5, 0, 0), with 100% occupancy, $B_{\text{iso}}(\text{Sr}) = 0.47(5) \text{ \AA}^2$, $B_{\text{iso}}(\text{Fe}) = 0.47(4) \text{ \AA}^2$, $B_{\text{iso}}(\text{O}) = 0.79(5)$, $R_p = 3.82\%$, $R_{\text{wp}} = 4.70\%$, $\chi^2 = 3.18$, $R_{\text{Bragg}} = 4.19\%$, $R_{\text{mag}} = 9.19\%$ (see Methods for definitions). **b**, The magnetic structure with a $2a_p \times 2a_p \times 2c_p$ magnetic unit cell of sides of length a , b and c , where iron sites are drawn. Arrows denote the direction of the magnetic moment.

The temperature variations of the magnetic NPD peak intensity and the hyperfine field nicely coincide with each other (see Fig. 3a and c, and Supplementary Table 1), giving the Néel temperature $T_N = 473$ K. The quadrupole interaction appearing in the magnetically split Mössbauer spectrum, which is equal to $S_1 - S_2$ in Fig. 3b, is almost temperature-independent (for example, 1.16 mm s^{-1} at 285 K), and is very close to the quadrupole splitting in the paramagnetic state, ΔE (Fig. 3b), of 1.06 mm s^{-1} . This proximity and the fact that the electric field gradient is uniaxial along the c axis by symmetry indicated that the magnetic hyperfine field lies in the a - b plane²³, consistent with the NPD results.

In spite of the apparent two-dimensionality in magnetism, the T_N is considerably higher than that (~ 200 K) of FeO having the rock-salt-type, three-dimensionally extended linear Fe-O-Fe bonding. This shows that SrFeO₂ has fairly large in-plane exchange constants

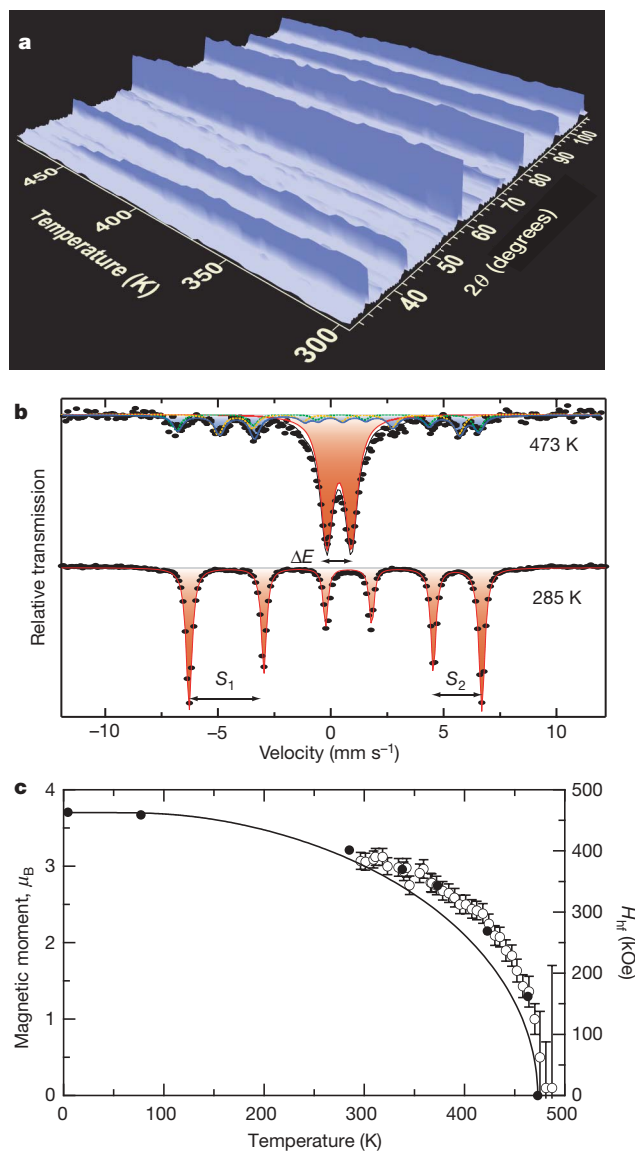


Figure 3 | Temperature evolution of the magnetic order in SrFeO₂. **a**, The *in situ* NPD profiles upon warming. The peak at $2\theta = 36^\circ$ corresponds to the $(1/2, 1/2, 1/2)$ magnetic reflection. **b**, Mössbauer spectra at 285 and 473 K. The red lines indicate the spectra from SrFeO₂, while the blue line at 473 K represents the spectrum from a small amount of SrFeO_{2.5}. The black line is the total fit. **c**, Temperature dependence of the magnetic moment and the hyperfine field H_{hf} determined by NPD (open circles) and Mössbauer spectroscopy (solid circles), respectively. The solid curve is the theoretical Brillouin function for $S = 2$. Error bars are s.d., determined by the Rietveld refinement.

owing to strong in-plane Fe $d_{x^2-y^2}$ to O p_{xy} hybridization. Another aspect of the strong hybridization is the isomer shift ($\sim 0.5 \text{ mm s}^{-1}$ at room temperature), which is located in the extreme covalent limit for a high-spin divalent iron²³. We also point out that the electronic configuration should be a twofold orbital degenerate ground state of $(d_{xz}, d_{yz})^3$ (ref. 1), because all iron atoms in SrFeO₂ are in a high-spin state with D_{4h} point symmetry. Remarkably, SrFeO₂ is free from instabilities such as orbital ordering or Jahn-Teller distortion even at the temperatures of 10 and 4.2 K, as derived from NPD and Mössbauer spectroscopy, respectively. We believe that the orbital instability is overcome by the extremely strong covalency that favours directional and symmetrical Fe-O bonding. Therefore, by applying the present synthetic approach to other iron oxides, such as conventional ferrites, we should be able to obtain novel magnetic materials containing Fe²⁺ ions in square-planar geometry and thus having greater magnetic anisotropy and higher transition temperatures.

SrFeO_{3-y} and related iron perovskite oxides have been intensely studied, because they exhibit fast oxygen transport combined with high electron conductivity even at low temperatures¹⁷. They are thus potential candidates for applications as electrodes for solid oxide fuel cells and batteries²⁴, membranes for oxygen separation²⁵ and electrocatalysis²⁶ and gas sensors²⁷. In addition, their unusual properties include aspects of vacancy orderings (at $y = 0, 0.125, 0.25$ and 0.5)¹⁵⁻¹⁷, charge disproportionation²⁸, giant magnetoresistance²⁹, helical antiferromagnetic spin structure³⁰, and high-spin to low-spin transition²⁸. Here we have shown that the reduction of SrFeO_{2.875} does not necessarily stop at the brownmillerite structure SrFeO_{2.5}, but goes beyond this stoichiometry to form a terminal phase with an infinite number of FeO₂ layers. This means that CaH₂ can provide a balanced reducing potential high enough to produce SrFeO₂ but not so high that it would result in over-reduction to Fe metal. Starting from SrFeO_{3-y}, a one-day reaction in the ranges $473 \text{ K} < T < 523 \text{ K}$, $523 \text{ K} < T < 673 \text{ K}$ and $673 \text{ K} < T$ produces SrFeO_{2.5}, SrFeO₂ and SrO-Fe mixture, respectively, whereas a one-week reaction at 473 K yields only SrFeO₂, demonstrating ever more control of reducing power by varying synthetic temperature and time.

We note that the reduction from SrFeO_{2.5} to SrFeO₂ is not a naive topotactic reduction because it involves the filling of the originally vacant sites within the tetrahedral layers of SrFeO_{2.5}. Upon heating in an oxygen atmosphere of 0.1 MPa, an opposite reaction back up to SrFeO_{2.875} via SrFeO_{2.5} takes place (Supplementary Fig. 4). Surprisingly, both the reduction and the oxygen uptake proceed at temperatures as low as ~ 400 K. This implies not only that oxygen is highly mobile in solids at low temperatures, but also that a given dense framework can rearrange towards new oxygen-ordered structures, which may be useful for solid oxide fuel cells, oxygen membranes and sensor materials oriented towards the reduction of working temperatures. It may also be of interest to investigate hole- or electron-doping into the infinite-layer FeO₂ sheets—for example, by introducing selectively apical oxygen atoms or by replacing Sr sites with a monovalent metal like Na.

METHODS SUMMARY

The reduction of SrFeO_{2.875} was performed using CaH₂ as a reducing agent, as described for LaSrCoO₄ (ref. 3). SrFeO_{2.875} and a two-molar excess of CaH₂ were finely ground in an Ar-filled glove box, sealed in an evacuated Pyrex tube, and reacted at 553 K for two days. The residual CaH₂ and the CaO byproduct were removed from the final reaction phase by washing them out with a NH₄Cl/methanol solution. Chemical analyses were based on EDS and thermogravimetry. The synchrotron powder XRD experiment was performed on the large Debye-Scherrer camera installed at the SPring-8 beam line BL02B2 by using an imaging plate as a detector. The wavelength of the X-ray is 0.77747 \AA . *Ex situ* NPD studies were carried out on the D1A diffractometer, installed at the Institute Laue Langevin. The wavelength of $\lambda = 1.91 \text{ \AA}$ was used. The *in situ* NPD profiles upon warming in dynamic vacuum was carried out on the D1B diffractometer installed at the Institute Laue Langevin, where $\lambda = 2.52 \text{ \AA}$ was used. ⁵⁷Fe Mössbauer spectra were taken under dynamical vacuum using a ⁵⁷Co/Rh source and a control absorber of α -Fe.

Full Methods and any associated references are available in the online version of the paper at www.nature.com/nature.

Received 3 July; accepted 5 October 2007.

- Wells, A. F. *Structural Inorganic Chemistry* 3rd edn (Oxford Univ. Press, Oxford, UK, 1962).
- Hayward, M. A. & Rosseinsky, M. J. Anion vacancy distribution and magnetism in the new reduced layered Co(II)/Co(I) phase $\text{LaSrCoO}_{3.5-x}$. *Chem. Mater.* **12**, 2182–2195 (2000).
- Hayward, M. A. *et al.* The hydride anion in an extended transition metal oxide array: $\text{LaSrCoO}_3\text{H}_{0.7}$. *Science* **295**, 1882–1884 (2002).
- Blundred, G. D., Bridges, A. B. & Rosseinsky, M. J. New oxidation states and defect chemistry in the pyrochlore structure. *Angew. Chem. Intl Edn* **43**, 3562–3565 (2004).
- Siegrist, T., Zahurak, S. M., Murphy, D. W. & Roth, R. S. The parent structure of the layered high-temperature superconductors. *Nature* **334**, 231–232 (1988).
- Takano, M., Takeda, Y., Okada, H., Miyamoto, M. & Kusaka, T. ACuO_2 (A: alkaline earth) crystallizing in a layered structure. *Physica C* **159**, 375–378 (1989).
- Smith, M. G., Manthiram, A., Zhou, J. & Goodenough, J. B. Electron-doped superconductivity at 40 K in the infinite-layer compound $\text{Sr}_{1-y}\text{Nd}_y\text{CuO}_2$. *Nature* **351**, 549–551 (1991).
- Azuma, M., Hiroi, Z., Takano, M., Bando, Y. & Takeda, Y. Superconductivity at 110 K in the infinite-layer compound $(\text{Sr}_{1-x}\text{Ca}_x)_{1-y}\text{CuO}_2$. *Nature* **356**, 775–776 (1992).
- Crespin, M., Levitz, P. & Gatinneau, L. Reduced forms of LaNiO_3 perovskite. 1. Evidence for new phases: $\text{La}_2\text{Ni}_2\text{O}_5$ and LaNiO_2 . *J. Chem. Soc. Faraday Trans. 2*, 1181–1194 (1983).
- Hyde, B. G. & Andersson, S. *Inorganic Crystal Structure* Ch. 15 (John Wiley & Sons, New York, 1989).
- Berry, J. F. *et al.* An octahedral coordination complex of iron(VI). *Science* **312**, 1937–1941 (2006).
- Bouwkamp, M. W., Bowman, A. C., Lobkovsky, E. & Chirik, P. J. Iron-catalyzed $[2\pi + 2\pi]$ cycloaddition of α,ω -dienes: the importance of redox-active supporting ligands. *J. Am. Chem. Soc.* **128**, 13340–13341 (2006).
- Hazen, R. M. & Burnham, C. W. The crystal structures of gillespite I and II: a structural determination at high pressure. *Am. Mineral.* **59**, 1166–1176 (1974).
- Leinenweber, K., Linton, J., Navrotsky, A., Fei, Y. & Parise, J. B. High-pressure perovskites on the join CaTiO_3 - FeTiO_3 . *Phys. Chem. Mineral.* **22**, 251–258 (1995).
- Takeda, Y. *et al.* Phase relation in the oxygen nonstoichiometric system SrFeO_x ($2.5 \leq x \leq 3$). *J. Solid-State Chem.* **63**, 237–249 (1986).
- Hodges, J. P. *et al.* Evolution of oxygen-vacancy ordered crystal structures in the perovskite series $\text{Sr}_n\text{Fe}_n\text{O}_{3n-1}$ ($n = 2, 4, 8$, and ∞), and the relationship to electronic and magnetic properties. *J. Solid-State Chem.* **151**, 190–209 (2000).
- Grenier, J.-C. *et al.* Electrochemical oxygen intercalation into oxide networks. *J. Solid-State Chem.* **96**, 20–30 (1992).
- Hayashi, N., Terashima, T. & Takano, M. Oxygen-holes creating different electronic phases in Fe^{4+} -oxides: successful growth of single crystalline films of SrFeO_3 and related perovskites at low oxygen pressure. *J. Mater. Chem.* **11**, 2235–2237 (2001).
- Hayward, M. A. Structural and magnetic properties of topotactically reduced $\text{YSr}_2\text{Mn}_2\text{O}_{7-x}$ ($0 < x < 1.5$). *Chem. Mater.* **18**, 321–327 (2006).
- Poltavets, V. V. *et al.* $\text{La}_3\text{Ni}_2\text{O}_6$: a new double T'-type nickelate with infinite $\text{Ni}^{1+/2+}\text{O}_2$ layers. *J. Am. Chem. Soc.* **128**, 9050–9051 (2006).
- Hayward, M. A. Phase separation during the topotactic reduction of the pyrochlore $\text{Y}_2\text{Ti}_2\text{O}_7$. *Chem. Mater.* **17**, 670–675 (2005).
- Hayward, M. A., Green, M. A., Rosseinsky, M. J. & Sloan, J. Sodium hydride as a powerful reducing agent for topotactic oxide deintercalation: synthesis and characterization of the nickel(I) LaNiO_2 . *J. Am. Chem. Soc.* **121**, 8843–8854 (1999).
- Greenwood, N. N. & Gibb, T. C. *Mössbauer Spectroscopy* Ch. 3 & 5 (Chapman and Hall, London, 1971).
- Shao, Z. & Haile, S. M. A high-performance cathode for the next generation of solid-state fuel cells. *Nature* **431**, 170–173 (2004).
- Sammells, A. F., Schwartz, M., Mackay, R. A., Barton, T. F. & Peterson, D. R. Catalytic membrane reactors for spontaneous synthesis gas production. *Catal. Today* **56**, 325–328 (2000).
- Badwal, S. P. S. & Ciacchi, F. T. Ceramic membrane technologies for oxygen separation. *Adv. Mater.* **13**, 993–996 (2001).
- Wang, Y., Chen, J. & Wu, X. Preparation and gas-sensing properties of perovskite-type SrFeO_3 oxide. *Mater. Lett.* **49**, 361–364 (2001).
- Takano, M. *et al.* Pressure-induced high-spin to low-spin transition in CaFeO_3 . *Phys. Rev. Lett.* **67**, 3267–3270 (1991).
- Battle, P. D. *et al.* Magnetoresistance in high oxidation state iron oxides. *Chem. Commun.* **767**, 987–988 (1998).
- Mostovoy, M. Helicoidal ordering in iron perovskite. *Phys. Rev. Lett.* **94**, 137205 (2005).

Supplementary Information is linked to the online version of the paper at www.nature.com/nature.

Acknowledgements We thank Y. Kiuchi, H. Ueda, M. Isobe and Y. Ueda for their help in EDS and thermogravimetric measurements and K. Kato for his help in the synchrotron X-ray experiments at SPring-8. This work was supported by Young Scientists A (H.K.), the Grant-in-Aid for Scientific Research on Priority Areas (H.K. and K.Y.) and Scientific Research S (M.T.) from MEXT. See the Supplementary Notes for more details.

Author Contributions H.K. designed the study in collaboration with W.P., with M.T.'s help; C.T. performed the initial synthesis and proposed the structural model; Y.T. and T.W. optimized the synthetic conditions, performed chemical characterizations, X-ray diffraction measurements and corresponding structural refinement; N.H. conducted the Mössbauer experiment, with M.T.'s help; M.C., C.R. and W.P. performed the neutron diffraction measurements and M.C. and W.P. performed the corresponding structural refinement; All the authors discussed the results; H.K. wrote the manuscript, with comments mainly from M.T. and W.P.

Author Information Atomic coordinates and structure factors for the crystal structure of SrFeO_2 have been deposited with the ICSD database under accession codes 418603, 418605 and 418606. Reprints and permissions information is available at www.nature.com/reprints. Correspondence and requests for materials should be addressed to H.K. (kage@kuchem.kyoto-u.ac.jp).

METHODS

A precursor $\text{SrFeO}_{2.875}$ ($y \approx 0.125$) was prepared by a conventional high-temperature ceramic method from predried SrCO_3 (99.99%) and Fe_2O_3 (99.99%). Stoichiometric amounts of SrCO_3 and Fe_2O_3 were ground together, heated at 1,273 K in air, ground again, and heated for an additional 24 h at 1,473 K. The reduction of $\text{SrFeO}_{2.875}$ was performed using CaH_2 as a reducing agent. $\text{SrFeO}_{2.875}$ (0.45 g) and a two-molar excess of CaH_2 (0.2 g) were finely ground in an Ar-filled glove box, sealed in an evacuated Pyrex tube (volume 15 cm^3) with a residual pressure less than 1.3×10^{-8} MPa, and reacted at 553 K for two days. The residual CaH_2 and the CaO byproduct were removed from the final reaction phase by washing them out with 0.1 M NH_4Cl in dried methanol.

The EDS experiments were carried out for the precursor and the final product using a JEOL (JSM-5600) scanning electron microscope equipped with an EDAX (Oxford Link ISIS) microanalytical system. Thermogravimetric measurements were performed using a Mac Science thermal analyser (TG-DTA2000). Measurements to analyse re-oxidation behaviour of SrFeO_2 were performed on a sample of around 20 mg that was rapidly loaded into an aluminium crucible and then heated at 10 K min^{-1} under flowing O_2 (0.1 MPa). Before the experiment, the sample was dried at 373 K for about 1 hour. The identity and oxygen stoichiometry of the re-oxidized products were determined by XRD.

The synchrotron powder diffraction experiment was performed on the large Debye–Scherrer camera installed at SPring-8 BL02B2 by using an imaging plate as a detector. Incident beams from a bending magnet were monochromatized to 0.77747 \AA . The sample was contained in a glass capillary tube with an inner diameter of 0.1 mm and was rotated during measurements. The synchrotron X-ray diffraction data were collected at room temperature in a 2θ range from 1° to 75° with a step interval of 0.01° .

The *ex situ* neutron powder diffraction studies were carried out on the D1A diffractometer, installed at the Institute Laue Langevin (Grenoble, France). A 200 mg sample sealed in a He-filled vanadium can was used and a wavelength of $\lambda = 1.91 \text{ \AA}$ was used. The *in situ* neutron powder diffraction experiments of SrFeO_2 upon warming in dynamic vacuum ($p_{\text{O}_2} < 1.3 \times 10^{-10}$ MPa) were carried out using the Institute Laue Langevin vacuum furnace on the D1B diffractometer installed at Institute Laue Langevin, where $\lambda = 2.52 \text{ \AA}$ was used. The temperature was varied from 270 to 500 K with a 0.5 K min^{-1} ramp rate. The temperature stability and average temperature were determined using a thermocouple placed at the sample position.

Mössbauer spectra of SrFeO_2 were taken under a dynamical vacuum, and the data were collected in transmission geometry by using a $^{57}\text{Co/Rh}$ γ -ray source at low temperature in combination with a constant-acceleration spectrometer. The source velocity was calibrated by using pure α -Fe as a control material. The low temperature measurements were carried out using a cryostat, while the high-temperature spectra were taken with a small amount of CaH_2 that was mixed with the SrFeO_2 powder to minimize re-oxidation of SrFeO_2 into the brownmillerite phase $\text{SrFeO}_{2.5}$ upon being heated. The obtained spectra were fitted by a lorentzian function. The subspectrum of $\text{SrFeO}_{2.5}$ observed at high temperatures was compared with that of ref. 31.

The X-ray and neutron diffraction patterns were analysed by the Rietveld method using the RIETAN 2000 (ref. 32) and FULLPROF software³³, respectively. The agreement indices used were the profile, $R_p = \sum |y_{io} - y_{ic}| / \sum y_{io}$, weighted profile, $R_{wp} = [\sum w_i (y_{io} - y_{ic})^2 / \sum w_i (y_{io})^2]^{1/2}$ and the goodness of fit, $\chi^2 = [R_{wp} / R_{exp}]^2$ where $R_{exp} = [(N - P) / \sum w_i (y_{io})^2]^{1/2}$, y_{io} and y_{ic} are the observed and calculated intensities, w_i is the weighting factor, N is the total number of y_{io} data when the background is refined, and P is the number of adjusted parameters. R_{Bragg} and R_{mag} are the R factors, $\sum |I_{ko} - I_{kc}| / \sum I_{ko}$, for nuclear and magnetic peaks, respectively, where I_{ko} and I_{kc} are the observed and calculated integrated intensity. B_{iso} is the isotropic temperature factor. The bond valence sum method was applied to estimate the valence of cations using tabulated parameters³⁴.

31. Adler, P. *et al.* Structural phase transition in $\text{Sr}_2\text{Fe}_2\text{O}_5$ under high pressure. *J. Solid-State Chem.* **155**, 381–388 (2000).
32. Izumi, F. & Ikeda, T. Rietveld-analysis program RIETAN-98 and its applications to zeolites. *Mater. Sci. Forum* **321–324**, 198–203 (2000).
33. Rodríguez-Carvajal, J. Recent advances in magnetic-structure determination by neutron powder diffraction. *J. Phys. B* **192**, 55–69 (1993).
34. Brown, I. D. & Altermatt, D. Bond-valence parameters obtained from a systematic analysis of the inorganic crystal structure database. *Acta Crystallogr. B* **41**, 244–247 (1985).